

# Calculation of immobilized enzyme reaction progress curves from nested ordered-sequential rate expressions

Peter Irwin,\* Janine Brouillette\*, Markus Germann,† Kevin Hicks,\* Michael Kurantz,\* and William Damert\*

\*Eastern Regional Research Center, ARS, USDA, Wyndmoor, PA, USA; and †Thomas Jefferson University, Kimmel Cancer Institute, NMR Laboratory, Bluemle Life Sciences Bldg., Room 815, 233 South 10th Street, Philadelphia, PA, USA

A method for estimating immobilized enzyme reaction progress curves, using simultaneous non-linear regression analysis of 2–3 substrate concentrations with time, is presented. These facile procedures involve using nested Gauss–Newton curve fitting algorithms on a Microsoft EXCEL spreadsheet. We refer to our technique as “nested” because the analysis consists of two or three mutually parameter-dependent sets of computations associated with bi- or termolecular enzyme-catalyzed reactions, respectively. We have applied the method to immobilized glucose oxidase-catalyzed reactions ( $[D\text{-glucose}]$  and  $[O_2]$  with time) and found that the kinetic parameters from initial velocity data were similar to those determined by the nested curve fitting method discussed herein. © 1999 Elsevier Science Inc. All rights reserved.

**Keywords:** Reaction progress curve; glucose oxidase; enzyme kinetics; enzyme immobilization; glucono- $\delta$ -lactone; gluconic acid; *Aspergillus niger*;  $^{13}\text{C}$ -NMR

## Introduction

Glucose oxidase (GO;  $\beta$ -D-glucose: $O_2$  1-oxidoreductase) is a flavin-adenine dinucleotide (FAD) modulated, cell wall-bound<sup>1</sup> glycoprotein.<sup>2–4</sup> This commercially important enzyme<sup>3,5–13</sup> catalyses (Figure 1) the oxidation of  $\beta$ -D-glucose's (G) anomeric carbon to form glucono- $\delta$ -lactone<sup>4,5,14–17</sup> which spontaneously hydrolyses to form gluconic acid (GA), an important product in the food and pharmaceutical industries.<sup>18</sup> The reaction mechanism of GO is best modeled<sup>19</sup> as an alternating two reactant, ordered-sequential, system frequently referred to as bi–bi (two substrates and two products) ping-pong (PP) because the enzyme's pro-

thetic group, FAD, fluctuates between two oxidation states.<sup>15–17,20–22</sup>

Standard GO PP kinetic techniques<sup>19–23</sup> rely on the observation of pseudo-zero order rate constants ( $\rho$ ) determined at various concentrations of the two substrates, glucose and  $O_2$  ( $[G]$  and  $[O_2]$ ; Figure 1).<sup>19</sup>

$$\begin{aligned} \rho &= \frac{\partial[GA]}{\partial t} = -\frac{\partial[G]}{\partial t} \\ &= \frac{V_{\max}^G [G][O_2]}{K_G [O_2] + K_{O_2} [G] + [G][O_2]} \\ &= \frac{V_{\max}^G}{\frac{K_G}{[G]} + \frac{K_{O_2}}{[O_2]} + 1} \end{aligned} \quad (1a)$$

$$K_G = \frac{k_2 + k_3}{k_1} \quad (1b)$$

Address reprint requests to Dr. Peter Irwin, USDA/ARS/ERRC, 600 E. Mermaid Lane, Wyndmoor, PA 19038, USA

Received 3 August 1998; revised 10 December 1998; accepted 14 December 1998

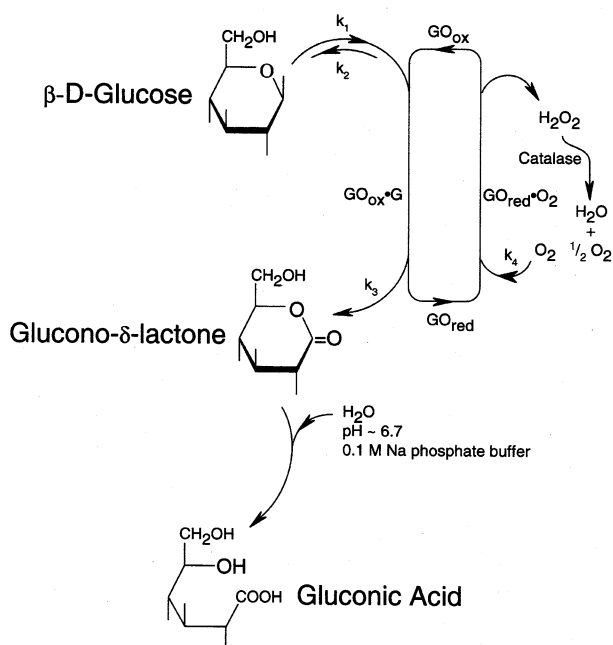


**Figure 1** Reaction scheme for the conversion of  $\beta$ -D-glucose to glucono- $\delta$ -lactone via GO

$$K_{O_2} = \frac{k_3}{k_4} \quad (1c)$$

$$V_{\max}^G = k_2[GO]_o \quad (1d)$$

In these equations, assuming only “weak” lactone inhibition,<sup>15</sup>  $K_G$  and  $K_{O_2}$  represent the substrate concentrations for which the average vacancy time equals the mean residence time of the GO<sub>red</sub>·G and GO<sub>ox</sub>·O<sub>2</sub> complexes, respectively.<sup>23</sup>

A facile reaction progress curve-fitting routine, which estimates kinetic parameters for multiple substrates, could be useful for immobilized enzymes for diverse reasons. Pseudo-zero order kinetic techniques require numerous independent observations of  $\rho$  as a function of the primary substrate concentration (with at least two secondary and tertiary substrate concentrations) and are not readily applicable for immobilized enzymes.<sup>13</sup> We have found that, because of sampling error associated with a hydrated solid, the utilization of substrate saturation kinetics with immobilized enzymes results in unsatisfactory scatter. Additionally, for the production of aldonic acids using immobilized enzymes such as glucose (EC 1.1.3.4) or hexose oxidase (EC 1.1.3.5), it is desirable to be able to predict the yield of the product, or loss of substrate, directly (e.g., concentration vs. time  $\equiv$  reaction progress curve). For such an analysis it is useful to know the values of  $K_G$  and  $K_{O_2}$  because changes in these parameters could occur due to the immobilization matrix<sup>24</sup> and alter the reaction progress curve. For instance, Gentry *et al.*<sup>23</sup> have shown that restricting an enzyme to any surface can alter the enzyme-substrate collision rate through perturbations in the “dimensionality of the diffusive path”. This finding implies that the surface structure can either in-

crease or decrease the effective substrate concentration which the immobilized enzyme encounters, depending on the chemical nature of the matrix used<sup>23,24</sup> and would, by definition, alter the apparent values of  $K_G$  and  $K_{O_2}$ . In order to model an immobilized GO-glucose reaction progress curve, and simultaneously extract the kinetic parameters, one must integrate the PP rate expression [Eq. (1a)].

$$-V_{\max}^G \int_0^t dt = \int_{[G]_0}^{[G]} \frac{K_G[O_2] + K_{O_2}[G] + [G][O_2]}{[G][O_2]} d[G] \quad (2a)$$

$$-V_{\max}^G t = \frac{\{[G] - [G]_0\} \{K_{O_2} + [O_2]\}}{[O_2]} + K_G \log_e \frac{[G]}{[G]_0} \quad (2b)$$

Eq. (2b) shows that it is impossible to gather all the primary substrate,  $[G]$  and  $[G]_0$ , concentration terms on one side of the definite integral since the solution involves a transcendental function of  $[G]$  in an essentially non-algebraic way. Thus, as shown previously,<sup>25</sup> algebraic considerations restrict the application of symbolic integration.

There are two types of reaction progress curve analysis:<sup>26</sup> integral methods<sup>25,27-38</sup> and differential methods.<sup>26,38-43</sup> We concern ourselves here only with the integral methods which tend to present fewer technical difficulties.<sup>39</sup> In simple systems (e.g., one substrate only), some integration methods<sup>27,43,44</sup> have employed analysis of mathematically-manipulated substrate concentration as a function of time using a symbolically integrated Michaelis-Menton<sup>21</sup> (MM) rate expression. Another technique<sup>28</sup> has been developed to address some of the errors associated with certain MM integration schemes and allows the utilization of simple regression analysis. However, the use of any linear regression technique for non-linear functions is problematic because they can be based on an incorrect error model.<sup>45</sup> Other methods, involving symbolically-integrated rate expressions, have also been proffered.<sup>25,27-37</sup> For instance, Duggleby and Morrison<sup>25,29</sup> developed a method which resulted in admirable reaction progress curve fits in various systems. However, for systems of high molecularity this method would require data to be collected at several concentrations for each substrate involved.

In this manuscript we describe a novel and facile numerical approach. The major difference between our approach and other numerically-integrated methods resides in our utilization of *nested* non-linear regression algorithms for each substrate to extract all the PP kinetic information as well as predict reaction progress curves. One advantage of our approach is that only two sets of observations, one for each substrate, are required. We refer to this technique as “nested” since it consists of two mutually parameter-dependent sets of X-Y vectors (for GO:  $[G]$  and  $[O_2]$  as a function of time) associated with each bi-molecular reaction

progress curve. Our method can be easily modified to work with higher order (e.g., termolecular) reaction mechanisms as well.

## Materials and methods

### Immobilization of GO

Numerous routines for immobilizing GO have been reported.<sup>3,7,8,10,11,46,47</sup> We have chosen to use Fractogel because it is a commercially available method for immobilizing manifold proteins especially for affinity chromatographic applications. Fractogel immobilization has the advantage over other methods since the gels' particle size is small (25–40  $\mu\text{m}$ ). Particle size is of particular concern;<sup>24</sup> if the ratio of the coefficient of diffusion for some substrate ( $S$ ) to the square of the unstirred layer ( $\delta$ ) surrounding an immobilizing matrix is  $\leq V_{\text{max}}^S/K_S$ , the reaction will be under diffusional control by the substrate. Clearly, if the particle size of the immobilizing matrix is small so will be  $\delta$ . Lastly, the immobilization procedure described herein is simple relative to more involved techniques.<sup>9,13,48–50</sup>

Typically 1 g of dry Fractogel (Fractogel EMD Azlactone 650S, 10087-1, EM Separations Technology, EM Industries, 480 S. Democrat Road, Gibbstown, NJ, USA 08027) was washed with 10 ml of 0.1 M Na phosphate (equimolar mono- and dibasic) buffer at a pH of approximately 6.7 and centrifuged to pellet the matrix. Approximately 10,000–20,000 units (1 unit  $\equiv$  1  $\mu\text{mol min}^{-1}$ ) of low catalase GO (Sigma, from *Aspergillus niger*; dialyzed and freeze-dried prior to use) was dissolved in 10 ml of buffer and added to the washed Fractogel whereupon the pH was readjusted. This mixture was agitated continuously and allowed to react for a total of 5–6 h at 25°C and refrigerated until needed. All Fractogel-GO immobilizations reported in this work were washed exhaustively until no free GO eluted.

### Assay methodology

All routine GO enzyme activity assays involved the use of  $\text{O}_2$ -saturated ( $[\text{O}_2]_0 \sim 0.00115 \text{ M}$ ) 1 M glucose ( $[\text{G}]_0$ ) in a water jacketed (1.42 ml; 25°C)  $\text{O}_2$  electrode/cell (YSI model 5300 Biological  $\text{O}_2$  monitor equipped with a Kipp & Zonon DELFT BV dual channel recorder) and non-linear regression analysis of the  $[\text{O}_2]$  vs. time progress curve utilizing a numerically-integrated version of the MM equation.<sup>21</sup> In these calculations, any  $m$ th  $[\text{O}_2]$  ( $[\text{O}_2]_m^{\text{calc}}$ ) was estimated to be

$$[\text{O}_2]_m^{\text{calc}} = [\text{O}_2]_{m-1}^{\text{obs}} - \frac{V_{\text{max}}^{\text{O}_2} \Delta t}{\frac{K_{\text{O}_2}}{[\text{O}_2]_{m-1}^{\text{obs}}} + 1} \quad (3)$$

at any time  $t_m$  ( $(m-1) \times \Delta t$ ); in Eq. (3)  $m > 1$  and  $[\text{O}_2]_1^{\text{calc}} = [\text{O}_2]_0$ ; the total number of points used ( $M$ ) was typically 21–41. Units of enzyme activity were obtained from  $V_{\text{max}}^{\text{O}_2}$  ( $\text{mol l}^{-1} \text{ s}^{-1}$ ) as

$$\text{units} = V_{\text{max}}^{\text{O}_2} \times 0.00142 \text{ l} \times 60 \text{ s min}^{-1} \times 10^6 \mu\text{mol mol}^{-1}. \quad (4)$$

Calculating activity in this fashion produced results similar to what was expected for GO from our source: Sigma estimated  $2.5 \times 10^5$  units  $\text{g}^{-1}$  dry GO;  $2.6 \times 10^5$  units  $\text{g}^{-1}$  was calculated [Eq. (4)] from the dialyzed and freeze-dried product. The apparent MM constant ( $K_{\text{O}_2}$ ) for  $\text{O}_2$  determined this way typically averaged 678 ( $\pm 30$ –40, asymptotic standard error,<sup>51</sup>  $\epsilon$ )  $\mu\text{M}$ .

$^{13}\text{C}$ -NMR spectroscopy was utilized for glucose quantification since gluconic acid was found to interfere with various reducing sugar assays. Samples (1 ml) for  $^{13}\text{C}$ -NMR analysis were dried under  $\text{N}_2$  and dissolved in 1 ml of 99.9 atom%  $\text{D}_2\text{O}$  (MSD isotopes;  $\text{pD} = \text{pH} + 0.4 \sim 7$ ) just prior to NMR examination. All samples reported herein were analyzed for glucose/gluconic acid with a Varian Gemini NMR spectrometer (5 mm dual  $^1\text{H}$ - $^{13}\text{C}$  probe) operated at approximately 200 MHz for  $^1\text{H}$  ( $B_0 = 4.7 \text{ T}$ ). The solutions were allowed to equilibrate approximately 15 min at 25–30°C whereupon manual shimming was performed with intermittent examination of the  $^1\text{H}$  spectrum to minimize residual  $\text{H}_2\text{O}$ 's  $\Delta\nu_{1/2}$  ( $\leq 2 \text{ Hz}$ ). Typical spectrometer conditions were: 4-K data points; 13-kHz spectral width; 18- $\mu\text{s}$  pulse width (approximately 68° pulse); approximately 2-s recycle time ( $T_{1\text{C}}$  for most simple sugar  $\text{C}_6$  resonances vary around 0.4 s); approximately 2,000 transients; 10-Hz line broadening (exponential multiplication).

Gluconic acid resonance assignments (6 mg of glucono- $\delta$ -lactone in 0.4 ml of 0.1 M Na phosphate [equimolar mono- and dibasic] in  $\text{D}_2\text{O}$ ) were made by performing various experiments on a Bruker AMX 600 NMR ( $B_0 = 14.09 \text{ T}$ ) spectrometer equipped with a 5-mm, triple resonance, inverse,  $z$ -gradient probe and a S-17 gradient amplifier (digital interface). All gradients were applied as 128 points (1/2-sine bell) for a duration of 1 ms (recovery delay = 20  $\mu\text{s}$ ). To make the  $^1\text{H}$  assignments, a gradient-assisted COSY experiment was acquired using a gradient pair applied at 6  $\text{G cm}^{-1}$ : one scan was recorded per  $t_1$  increment with a sweep width of 2.5 ppm for  $t_1$  and  $t_2$ ; 1 K of complex data points were acquired for the  $f_2$  dimension and 256 increments in  $f_1$ . Data were zero-filled to 512 points in  $t_1$  and further processed using sine bell apodization in both  $t_1$  and  $t_2$ . To assign the  $^{13}\text{C}$  spectrum, a phase sensitive HSQC experiment was performed using gradients for coherence pathway rejection:<sup>52</sup> gradients were applied at 18,  $-10.8$  and  $-3.6 \text{ G cm}^{-1}$ ; a sweep width of 6 ppm was used for  $^1\text{H}$  and 55 ppm for  $^{13}\text{C}$ ; one transient of 1-K complex data points were acquired for the 128  $t_1$  increments; GARP decoupling was applied during the acquisition period. The data was processed using a shifted-sine bell apodization function in  $t_1$  and  $t_2$  whereupon data were zero-filled to 512 points in  $t_1$  prior to fourier transformation; no base plane correction was applied. Glucose resonance assignments were based upon the work by Pfeffer *et al.*<sup>53</sup>

For NMR glucose quantification, the methylene hydroxyl, C-6, resonances of both glucose and gluconic acid were used. At the pH and ionic strength employed in these experiments neither  $\gamma$ - nor  $\delta$ -gluconolactone were apparent (Figure 2).  $[\text{G}]$  was calculated (Figure 2, inset) as

$$[\text{G}] = \frac{A_{\text{G}}}{A_{\text{G}} + A_{\text{GA}}} \times [\text{G}]_0 \quad (5)$$

following linear baseline correction ( $[\text{G}]_0 = 0.1$  or  $0.2 \text{ M}$ ). Figure 2 displays  $^{13}\text{C}$ -NMR spectra ( $t = 14, 28, 42, 56$  and  $182 \text{ min}$ ) of representative samples (GO type X-S immobilized on Fractogel: 38 units  $\text{g}^{-1}$ , approximately 1.59 g were used in a 25-ml reactor; apparent  $K_{\text{G}} = 64 \text{ mM}$ ). As the reaction times progressed from 14 to 182 min, gluconic acid's C-6 resonance

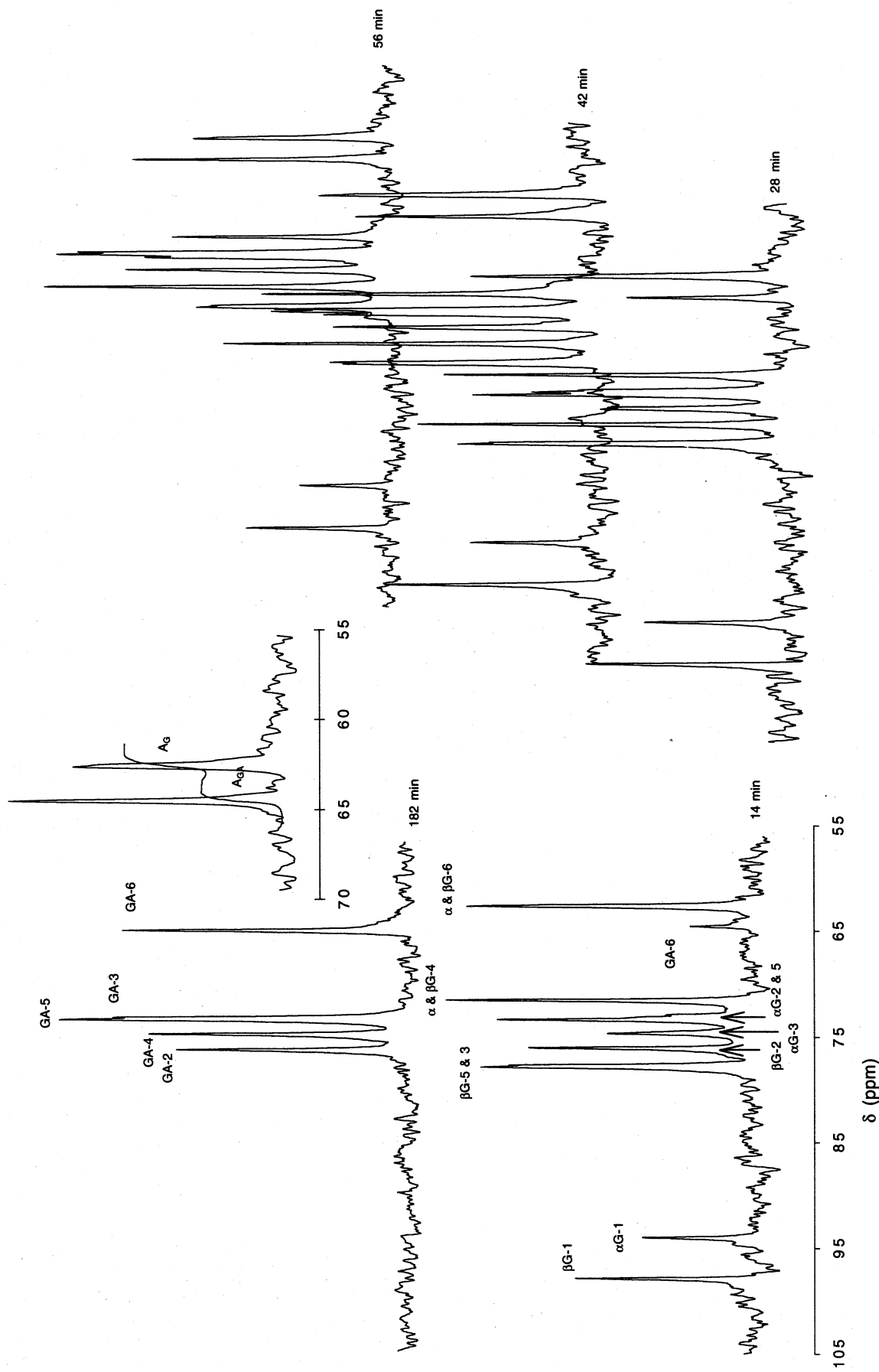


**Figure 2** Representative  $^{13}\text{C}$ -NMR spectra of Fractogel·GO reaction mixtures as a function of time. Resonance assignments are provided for both the 14 and 182 min (in the presence of Fractogel·GO: 0.1 M Na phosphate buffer) spectra. *Inset:* baseline corrected integral for the C-6 resonances of the 56-min spectrum

(GA-6: 64.5 ppm) gradually increased in extent at the expense of glucose's  $\alpha/\beta$ -C-6 resonance (62.7 ppm). We have performed 400 MHz  $^1\text{H}$  NMR studies on these same samples, integrating the H-1 or H-2 resonances for glucose or gluconic acid, respectively, with similar results but, due to requisite presaturation of  $\text{H}_2\text{O}$ , were concerned that the  $\alpha/\beta$ -H-1 resonances' integration might be affected.

### Immobilized GO reaction conditions

Secondary substrate ( $\text{O}_2$ ) reaction progress curve observations were made applying methods, aforementioned, using approximately 11–61 mg (pelleted wet weight) of the Fractogel·GO matrix without catalase. All primary substrate ( $[\text{G}]_0 = 0.1$  or  $0.2$  M) reaction progress curve studies ( $[\text{O}_2]_0 \sim 0.00115$  M in 25 ml of 0.1 M Na phosphate buffer, continuous agitation, pH 6.7 at  $25^\circ\text{C}$ ) were performed using approximately 0.75–1.76 g of hydrated Fractogel·GO with approximately 1,000 units of catalase (Sigma C-9322 Lot 84H7170). Specific reaction conditions are presented in the figure headings. Due to the continuous production of gluconic acid, the reactions were maintained at a constant pH ( $\bar{x} = 6.76 \pm 0.12$ ) with the addition of small (5–10  $\mu\text{l}$ ) aliquots of NaOH-saturated  $\text{H}_2\text{O}$  to a total of approximately  $170 \pm 40$   $\mu\text{l}$ . For the glucose experiments, 1 ml of sample was collected at each time interval, immediately centrifuged (Microfuge, 30 s) to pellet out solids and dried under  $\text{N}_2$ . The samples were redissolved in  $\text{D}_2\text{O}$  only just prior to  $^{13}\text{C}$ -NMR analysis. Several samples were maintained at room temperature (open to air) after NMR spectroscopic examination for future study; results indicated that there was no active Fractogel·GO in these solutions since the relative concentrations of glucose and gluconic acid remained constant.

All GO substrate saturation PP kinetic assays involved the use of air- or  $\text{O}_2$ -saturated ( $[\text{O}_2]_0 \sim 288$  or  $1150$   $\mu\text{M}$ , respectively) 0.1 M Na phosphate buffer with 0–100 mM D-glucose ( $[\text{G}]_0$ ) in a water jacketed (1.42 ml;  $25^\circ\text{C}$ )  $\text{O}_2$  electrode cell. Linear regression analysis of  $[\text{O}_2]$  vs. time data was performed in order to calculate initial velocity ( $\rho$ ). For the Fractogel·GO substrate saturation PP kinetic study, approximately  $12 \pm 3$  mg (approx. 0.45 units; 38 units of GO type X-S  $\text{g}^{-1}$ ) of the hydrated gel were used for each observation. For

solution studies 100  $\mu\text{l}$  (approx. 1.7 units) of GO (Sigma types: X-S or II) was allocated into the  $\text{O}_2$  electrode cell with a Hamilton syringe. Standard non-linear regression analysis using Eq. (1a) was used to extract the various kinetic parameters from  $\rho$  as a function of  $[\text{G}]_0$  at the two  $[\text{O}_2]_0$ s reported above.

### Reaction progress curve calculations

The computational procedure reported herein is identical to the any Gauss–Newton (GN) linearization procedure<sup>45,51</sup> with the exception that two sets of X–Y vectors ( $\text{X}^{\text{G}}\text{--Y}^{\text{G}}$  and  $\text{X}^{\text{O}_2}\text{--Y}^{\text{O}_2}$ ), and associated matrices, are put to use and iterated simultaneously. In the  $\text{X}^{\text{G}}\text{--Y}^{\text{G}}$  data arrays,  $K_{\text{O}_2}$  is treated as a constant and made equal to that same term in the  $\text{X}^{\text{O}_2}\text{--Y}^{\text{O}_2}$  set of computations. Concurrently, in the  $\text{X}^{\text{O}_2}\text{--Y}^{\text{O}_2}$  computations,  $K_{\text{G}}$  is treated as a constant and made commensurate with the  $K_{\text{G}}$  term being iteratively solved for in the  $\text{X}^{\text{G}}\text{--Y}^{\text{G}}$  set of arrays.

The method and algorithm presented in this work could, of course, be coded in any suitable language, such as FORTRAN or Mathematica. We chose to base our presentation on Microsoft EXCEL because it is one of the most widely utilized computational program which has built-in array functions with iterative solving. Additionally, manipulating arrays is much easier to do in EXCEL than it is with other data analysis packages, such as Mathematica, because EXCEL spreadsheets are arrays themselves. To demonstrate the EXCEL nested and numerically-integrated GN procedure we have created a simplified spreadsheet shown in Figure 3 (indices:  $l \cdots L = 2$ ,  $m \cdots M = 7$ ,  $n \cdots N$  for parameters, observed data, and iterations, respectively). For clarity we have kept the total number of points small ( $M = 7$ ). In order to construct the X–Y vectors, computer-generated points were created using the numerical functions for glucose and  $\text{O}_2$  shown in Table 1 whereupon  $M = 120$  ( $\Delta t = 1$ ). The values for  $Y_m^{\text{G}}$  and  $Y_m^{\text{O}_2}$  ( $M = 7$ ) were selected from this array at increments of  $\Delta t = 18$ . All the NMR and  $\text{O}_2$  electrode data discussed in this work involved similar manipulations. Herein,  $\mathbf{Z}^{45,51}$  represents the partial derivative matrix of  $F_m^{\text{G}}$  or  $F_m^{\text{O}_2}$  (Table 1; with respect to  $V_{\text{max}}^{\text{G}}$ ,  $K_{\text{G}}$ ,  $V_{\text{max}}^{\text{O}_2}$ ,  $K_{\text{O}_2}$ ) and  $\mathbf{Z}^l$

**Table 1** Arrays used in the evaluation of reaction progress curves utilizing numerically integrated, nested, biomolecular ordered-sequential rate expression

| $m$ | $X_m^{\text{G}} = \text{time (min)}$ | $F_m / \text{mol glucose l}^{-1}$   | $X_m^{\text{O}_2} = \text{time (s)}$ | $F_m / \text{mol O}_2 \text{ l}^{-1}$   |
|-----|--------------------------------------|---|--------------------------------------|---|
| 1   | $0 \times \Delta t$                  | $[\text{G}]_0 = Y_1^{\text{G}} = F_1$   | $0 \times \Delta t$                  | $[\text{O}_2]_0 = Y_1^{\text{O}_2} = F_1$   |
| 2   | $1 \times \Delta t$                  | $Y_1^{\text{G}} - \frac{V_{\text{max}}^{\text{G}} \Delta t}{\frac{K_{\text{G}}}{Y_1^{\text{G}}} + \frac{K_{\text{O}_2}}{[\text{O}_2]_0} + 1} = F_2$           | $1 \times \Delta t$                  | $Y_1^{\text{O}_2} - \frac{V_{\text{max}}^{\text{O}_2} \Delta t}{\frac{K_{\text{G}}}{[\text{G}]_0} + \frac{K_{\text{O}_2}}{Y_1^{\text{O}_2}} + 1} = F_2$         |
| 3   | $2 \times \Delta t$                  | $Y_2^{\text{G}} - \frac{V_{\text{max}}^{\text{G}} \Delta t}{\frac{K_{\text{G}}}{Y_2^{\text{G}}} + \frac{K_{\text{O}_2}}{[\text{O}_2]_0} + 1} = F_3$           | $2 \times \Delta t$                  | $Y_2^{\text{O}_2} - \frac{V_{\text{max}}^{\text{O}_2} \Delta t}{\frac{K_{\text{G}}}{[\text{G}]_0} + \frac{K_{\text{O}_2}}{Y_2^{\text{O}_2}} + 1} = F_3$         |
| ... | ...                                  | ...   | ...                                  | ...   |
| $M$ | $(M - 1) \times \Delta t$            | $Y_{M-1}^{\text{G}} - \frac{V_{\text{max}}^{[\text{G}]} \Delta t}{\frac{K_{\text{G}}}{Y_{M-1}^{\text{G}}} + \frac{K_{\text{O}_2}}{[\text{O}_2]_0} + 1} = F_M$ | $(M - 1) \times \Delta t$            | $Y_{M-1}^{\text{O}_2} - \frac{V_{\text{max}}^{\text{O}_2} \Delta t}{\frac{K_{\text{G}}}{[\text{G}]_0} + \frac{K_{\text{O}_2}}{Y_{M-1}^{\text{O}_2}} + 1} = F_M$ |

|    | A  | B               | C           | D         | E   | F               | G                 | H                   | I                         | J        | K |
|----|--|-----------------|-------------|-----------|---|-----------------|-------------------|---------------------|---------------------------|----------|---|
| 1  | t (min)                                      | $Y_m^G / M$     | $F_m^G$     |           | $V_{max}^G$   | $K_G$           | $V_{max}^{O_2}$   | $K_{O_2}$           | $SS_G$                    |          |   |
| 2  | 0  | 0.1             | 0.1         |           | 2.50E-03  | 2.50E-02        | 4.00E-05          | 7.00E-04            | 2.51E-05                  |          |   |
| 3  | 18   | 0.076249        | 0.075824    |           | $V_{max,n}^G$   | $K_{G,n}$       | $V_{max,n}^{O_2}$ | $K_{O_2,n}$         | $SS_{O_2}$                |          |   |
| 4  | 36   | 0.053706        | 0.0530436   |           | 2.50E-03  | 2.50E-02        | 4.00E-05          | 7.00E-04            | 5.74E-09                  |          |   |
| 5  | 54   | 0.03316         | 0.0320389   |           | $\Delta P$ for G (=MMULT(A30:G31,H6:H12))                 |                 |                   | $[Y_m^G - F_m]$     | $Z$ for [G]               |          |   |
| 6  | 72   | 0.016161        | 0.0141349   |           |   |                 | 0.000247          | 0                   | -9.67038                  | 0.129884 |   |
| 7  | 90   | 0.00522         | 0.001913    |           |   |                 | 0.015146          | 0.000425            | -9.28204                  | 0.156936 |   |
| 8  | 108  | 0.001053        | -0.001811   |           | $\Delta P$ for G (=MMULT(A43:G44,H14:H20))                |                 |                   | 0.000663            | -8.66698                  | 0.194257 |   |
| 9  | t (sec)                                      | $Y_m^{O_2} / M$ | $F_m^{O_2}$ |           | $\epsilon = \text{SQRT}((12*(A27 \text{ or } B28)/(7-2))$ |                 | 9.48E-06          | 0.001121            | -7.61013                  | 0.242568 |   |
| 10 | 0  | 0.001145        | 0.001145    |           |   |                 | 0.000496          | 0.002026            | -5.69935                  | 0.279152 |   |
| 11 | 18   | 0.000781        | 0.0007582   |           | 2.47E-04  | $V_{max}^G$     |                   | 0.003307            | -2.81231                  | 0.210429 |   |
| 12 | 36   | 0.000477        | 0.0004455   |           | 9.02E-03  | $K_G$           |                   | 0.002864            | -0.71001                  | 0.066488 |   |
| 13 | 54   | 0.000252        | 0.0002122   |           | $\epsilon = \text{SQRT}((14*(A40 \text{ or } B41)/(7-2))$ |                 |                   | $[Y_m^{O_2} - F_m]$ | $Z$ for [O <sub>2</sub> ] |          |   |
| 14 | 72   | 0.000113        | 7.33E-05    |           | 7.71E-06  | $V_{max}^{O_2}$ |                   | 0                   | -9.67038                  | 0.181497 |   |
| 15 | 90   | 4.48E-05        | 1.642E-05   |           | 2.93E-04  | $K_{O_2}$       |                   | 2.28E-05            | -8.38651                  | 0.200128 |   |
| 16 | 108  | 1.64E-05        | 2.131E-06   |           |   |                 |                   | 3.16E-05            | -6.62484                  | 0.204402 |   |
| 17 |  |                 |             |           |   |                 |                   | 4E-05               | -4.47035                  | 0.176147 |   |
| 18 |  |                 |             |           |   |                 |                   | 4.02E-05            | -2.42593                  | 0.115271 |   |
| 19 | Glucose Arrays                               |                 |             |           |   |                 |                   |                     |                           |          |   |
| 20 | $Z^T$ (=TRANSPOSE(I6:J12))                   |                 |             |           |   |                 |                   |                     |                           |          |   |
| 21 | -9.67E+00                                    | -9.28E+00       | -8.67E+00   | -7.61E+00 | -5.70E+00   | -2.81E+00       | -7.10E-01         |                     |                           |          |   |
| 22 | 1.30E-01                                     | 1.57E-01        | 1.94E-01    | 2.43E-01  | 2.79E-01  | 2.10E-01        | 6.65E-02          |                     |                           |          |   |
| 23 | $ZZ$ (=MMULT(A21:G22,I6:J12))                |                 |             |           |   |                 |                   |                     |                           |          |   |
| 24 | 3.54E+02                                     | -8.47E+00       |             |           |   |                 |                   |                     |                           |          |   |
| 25 | -8.47E+00                                    | 2.65E-01        |             |           |   |                 |                   |                     |                           |          |   |
| 26 | $(ZZ)^{-1}$ (=MINVERSE(A24:B25))             |                 |             |           |   |                 |                   |                     |                           |          |   |
| 27 | 1.21E-02                                     | 3.88E-01        |             |           |   |                 |                   |                     |                           |          |   |
| 28 | 3.88E-01                                     | 1.62E+01        |             |           |   |                 |                   |                     |                           |          |   |
| 29 | $(ZZ)^{-1} Z^T$ (=MMULT(A27:B28,A21:G22))    |                 |             |           |   |                 |                   |                     |                           |          |   |
| 30 | -6.69E-02                                    | -5.17E-02       | -2.97E-02   | 1.87E-03  | 3.93E-02  | 4.76E-02        | 1.72E-02          |                     |                           |          |   |
| 31 | -1.65E+00                                    | -1.06E+00       | -2.17E-01   | 9.76E-01  | 2.31E+00  | 2.32E+00        | 8.02E-01          |                     |                           |          |   |
| 32 | Oxygen Arrays                                |                 |             |           |   |                 |                   |                     |                           |          |   |
| 33 | $Z^T$ (=TRANSPOSE(I14:J20))                  |                 |             |           |   |                 |                   |                     |                           |          |   |
| 34 | -9.67E+00                                    | -8.39E+00       | -6.62E+00   | -4.47E+00 | -2.43E+00   | -1.07E+00       | -4.09E-01         |                     |                           |          |   |
| 35 | 1.81E-01                                     | 2.00E-01        | 2.04E-01    | 1.76E-01  | 1.15E-01  | 5.64E-02        | 2.27E-02          |                     |                           |          |   |
| 36 | $Z^T Z$ (=MMULT(A34:G35,I14:J20))            |                 |             |           |   |                 |                   |                     |                           |          |   |
| 37 | 2.35E+02                                     | -5.92E+00       |             |           |   |                 |                   |                     |                           |          |   |
| 38 | -5.92E+00                                    | 1.63E-01        |             |           |   |                 |                   |                     |                           |          |   |
| 39 | $(Z^T Z)^{-1}$ (=MINVERSE(A37:B38))          |                 |             |           |   |                 |                   |                     |                           |          |   |
| 40 | 5.18E-02                                     | 1.88E+00        |             |           |   |                 |                   |                     |                           |          |   |
| 41 | 1.88E+00                                     | 7.47E+01        |             |           |   |                 |                   |                     |                           |          |   |
| 42 | $(Z^T Z)^{-1} Z^T$ (=MMULT(A40:B41,A34:G35)) |                 |             |           |   |                 |                   |                     |                           |          |   |
| 43 | -1.59E-01                                    | -5.71E-02       | 4.21E-02    | 1.00E-01  | 9.16E-02  | 5.11E-02        | 2.16E-02          |                     |                           |          |   |
| 44 | -4.66E+00                                    | -8.49E-01       | 2.79E+00    | 4.74E+00  | 4.04E+00  | 2.21E+00        | 9.27E-01          |                     |                           |          |   |

**Figure 3** Microsoft EXCEL spreadsheet showing the computation of the various arrays used to analyze a nested set ([G] and [O<sub>2</sub>] vs. time) of reaction product data (a four parameter fit) and utilizing the GN linearization procedure

is the transpose of  $Z$ . All calculations (Figure 3) were performed by carrying out the following steps:

- (1) The X-Y vectors were defined:

$$X_m^G = \{A2:A8\} \text{ and } Y_m^G = \{B2:B8\}$$

$$X_m^{O_2} = \{A10:A16\} \text{ and } Y_m^{O_2} = \{B10:B16\}$$

- (2)  $F_{mn}^G = \{C2:C8\}$  and  $F_{mn}^{O_2} = \{C10:C16\}$

- (3) Cells {E2:H2} define  $V_{max}^G$ ,  $K_G$ ,  $V_{max}^{O_2}$ , and  $K_{O_2}$ , respectively. Cells {E4:H4} define:

$$V_{max,n}^G = V_{max}^G + (G6 \times \kappa) \quad (6a)$$

$$K_{G,n} = K_G + (G7 \times \kappa) \quad (6b)$$

$$V_{max,n}^{O_2} = V_{max}^{O_2} + (G9 \times \kappa) \quad (6c)$$

$$K_{O_2,n} = K_{O_2} + (G10 \times \kappa). \quad (6d)$$

The convergence rate factor,  $\kappa$ , was set to 0.1 in order to slow down the convergence process and thus avoid potential problems with overshooting<sup>51</sup> the desired minima in the error sum of squares. We chose this value of  $\kappa$  because it gave the best overall results and was based exclusively on trial-and-error; of course,  $\kappa$  can be unity when the initial estimates are fairly close to the final form.

- (4) Cells {H6} = 0 and {H7:H12} =

$$\{B3:B8\} - \left\{ \{B2:B7\} - \frac{V_{max}^G \Delta t}{\frac{K_G}{\{B2:B7\}} + \frac{K_{O_2}}{\$B\$10} + 1} \right\}. \quad (7a)$$

A simple reaction progress curve computational method: P. Irwin et al.

Cells {H14} = 0 and {H15:H20} =

$$\{B11:B16\} - \left( \{B10:B15\} - \frac{V_{\max}^{O_2} \Delta t}{\frac{K_G}{\$B\$2} + \frac{K_{O_2}}{\{B10:B15\}} + 1} \right) \quad (7b)$$

Equalities within brackets, “{}”, indicate that the expression is applied throughout a block of cells (e.g., an arrayed function); to enter an array function, all cells to be used must be selected (e.g., for A34:G35) and the equation input (e.g., = TRANSPOSE(I14:J20)) followed by “command” + “enter” (Macintosh version) or “control” + “shift” + “enter” (PC version). Cells defined as \$LETTER\$NUMBER indicate that each cell within the array contains this particular, or absolute, reference regardless of its position within an array. For example, when  $m = 2$

$$Y_2^G - F_{2n}^G = H7 = B3 - \left( B2 - \frac{V_{\max}^G \Delta t}{\frac{K_G}{B2} + \frac{K_{O_2}}{\$B\$10} + 1} \right) \quad (7c)$$

- (5) Cells I2 and I4 define the sums of squares for glucose and O<sub>2</sub>, respectively,

$$\begin{aligned} SS_G &= \{SUM((H6:H12)^2)\} \text{ and } SS_{O_2} \\ &= \{SUM((H14:H20)^2)\}, \end{aligned} \quad (8)$$

- (6) Cells {I6:I12} =

$$Z_{m1} \equiv \frac{\partial F_{mn}^G}{\partial V_{\max}^G} = - \frac{\Delta t}{1 + \frac{K_G}{\{B2:B8\}} + \frac{K_{O_2}}{\$B\$10}} \quad (9a)$$

Cells {J6:J12} =

$$Z_{m2} \equiv \frac{\partial F_{mn}^G}{\partial K_G} = \frac{V_{\max}^G \Delta t}{\{B2:B8\} \times \left( 1 + \frac{K_G}{\{B2:B8\}} + \frac{K_{O_2}}{\$B\$10} \right)^2} \quad (9b)$$

Cells {I14:I20} =

$$Z_{m1} \equiv \frac{\partial F_{mn}^{O_2}}{\partial V_{\max}^{O_2}} = - \frac{\Delta t}{1 + \frac{K_G}{\$B\$2} + \frac{K_{O_2}}{\{B10:B16\}}} \quad (9c)$$

Cells {J14:J20} =

$$Z_{m2} \equiv \frac{\partial F_{mn}^{O_2}}{\partial K_{O_2}} =$$

$$\frac{V_{\max}^{O_2} \Delta t}{\{B10:B16\} \times \left( 1 + \frac{K_G}{\$B\$2} + \frac{K_{O_2}}{\{B10:B16\}} \right)^2} \quad (9d)$$

- (7)  $Z^I$  (all arrays for glucose), {A21:G22}, was calculated by selecting the appropriate (2 × 7) cells and performing the function

$$\{ = \text{TRANSPOSE}(I6:J12) \} \quad (10a)$$

$Z^I Z$ , {A24:B25}

$$\{ = \text{MMULT}(A21:G22, I6:J12) \} \quad (10b)$$

$Z^I Z^{-1}$ , {A27:B28}

$$\{ = \text{MINVERSE}(A24:B25) \} \quad (10c)$$

$Z^I Z^{-1} Z^I$ , {A30:G31}

$$\{ = \text{MMULT}(A27:B28, A21:G22) \} \quad (10d)$$

- (8)  $Z^I$  (all arrays for O<sub>2</sub>), {A34:G35}

$$\{ = \text{TRANSPOSE}(I14:J20) \} \quad (11a)$$

$Z^I Z$ , {A37:B38}

$$\{ = \text{MMULT}(A34:G35, I14:J20) \} \quad (11b)$$

$Z^I Z^{-1}$ , {A40:B41}

$$\{ = \text{MINVERSE}(A37:B38) \} \quad (11c)$$

$Z^I Z^{-1} Z^I$ , {A43:G44}

$$\{ = \text{MMULT}(A40:B41, A34:G35) \} \quad (11d)$$

- (9) Generally, for any substrate  $S$  at some iterative state  $n$  for a  $M$  array of  $[S]$  observations

$$\Delta P = \begin{bmatrix} V_{\max}^S - V_{\max, n}^S \\ K_S - K_{S, n} \end{bmatrix} = (Z^I Z)^{-1} Z^I \begin{bmatrix} Y_1^S - F_{1n}^S \\ Y_2^S - F_{2n}^S \\ \dots \\ Y_M^S - F_{Mn}^S \end{bmatrix}; \quad (12a)$$

$\Delta P$  for glucose, {G6:G7}

$$\{ = \text{MMULT}(A30:G31, H6:H12) \} \quad (12b)$$

$\Delta P$  for O<sub>2</sub>, {G9:G10}

$$\{ = \text{MMULT}(A43:G44, H14:H20) \} \quad (12c)$$

Errors (E11, E12, E14, E15), known as the asymptotic standard error or  $\epsilon$ , related to the individual kinetic parameters can be estimated from the following formula whereupon

$$\varepsilon = \sqrt{\frac{(\mathbf{Z}/\mathbf{Z})_{ll}^{-1} \sum_{m=1}^M (Y_m - F_m)^2}{M - L}}; \quad (12d)$$

subscript  $ll$ , above, stands for the  $ll$ th (e.g., diagonal) element of the matrix  $(\mathbf{Z}/\mathbf{Z})^{-1}$ ; e.g., for  $K_G$ ,

$$E12 = \text{SQRT}(I2 * B28 / (7 - 2)); \quad (12e)$$

thus  $K_G = 25 \pm 9$  mM.

- (11) To select for iterative solving in EXCEL: choose either “preferences” or “options” (depending on version) from the “tools” menu → “calculation” → then choose “automatic” or “manual”, check the iteration box, set the “maximum iterations” (we use 500), and set the “maximum change” (we use 0.001). Lastly, cells {E2:H2} are made equal to {E4:H4} thus creating the circular reference needed to induce iterative solving (the precision desired can be altered by selecting the appropriate cells, {E2:H2} and {E4:H4}, and changing the number of decimal places desired). This is done by selecting cells {E2:H2} which have some initial value provided, press “=”, “down arrow” to the reference cells {E4:H4}, then “enter”; this process is repeated for each of the selected cells. The criteria used for establishing convergence is based upon observation of the minimization of the sums of squares of the observed differences between the fit and the data (e.g., I2 and I4). When the I2 & I4 no longer change in the last decimal place we can reasonably assume that the calculation has converged and can manually stop the process by typing in the displayed values for all the parameters. Another factor for the determination of convergence is change in the two  $\Delta P$  arrays, {G6:G7} and {G9:G10}. When these cells are changing very little relative to the values in {E2:H2} then one can also say the process has converged. Lastly, EXCEL will also stop the calculation when the maximum change parameter has been reached across the spreadsheet.

With any nested and numerically-integrated GN template as a starting point, approximately 10 min are required to modify the sheet for a new set of  $\mathbf{X}$ - $\mathbf{Y}$  vectors.

## Results and discussion

### Reaction progress curve modeling: computer-generated data

In *Figure 4* we present plots of computer-generated data as well as the initial ( $n = 0$ ) and final ( $N \sim 50$ ) fits using the nested and numerically-integrated GN procedure outlined in Section 2. In order to construct the  $\mathbf{X}$ - $\mathbf{Y}$  vectors in *Figure 4* the [G] and [O<sub>2</sub>] arrays were created using the numerical functions shown in *Table 1* whereupon  $M = 120$  ( $\Delta t = 1$ ). The values for  $Y_m^G$  and  $Y_m^{O_2}$  ( $\pm 5\%$  error;  $M = 41$ ) were selected from this array at increments of  $\Delta t = 3$  whereupon

$$Y_m^{\text{Error}} = Y_m + (Y_m \times [\text{RAND}() - \frac{1}{2}] \times 0.1); \quad (13)$$

the EXCEL function, RAND(), returns an evenly distributed random number  $\geq 0$  and  $< 1$ . In the table of initial/final estimates (*Figure 4*) the first row of numbers represent initial values which cause the reaction progress curve fits to undershoot the observed ( $U$ ), the second line of initial estimates cause the curves to overshoot ( $O$ ) the observed while the third has mixed ( $M$ ) values. Our algorithm converged to the shown lines of best fit in all cases which we tested and the converged parametric values varied only approximately  $-2$ – $6\%$  from those used to generate the data. We also have repeated this procedure for a termolecular reaction whereupon

$$\rho = -\frac{\partial[S_1]}{\partial t} = \frac{V_{\max}^{S_1}[S_1][S_2][S_3]}{K_{S_1}[S_2][S_3] + K_{S_2}[S_1][S_3] + K_{S_3}[S_1][S_2] + [S_1][S_2][S_3]}. \quad (14)$$

In these tests, the converged parameters deviated from the values used to generate the data only  $-1$ – $9\%$ . Thus, by independently observing three (for an termolecular reaction) sets of reaction progress data and utilizing the nested GN linearization procedure, a  $2 \times 3$  parameter fit is achieved with excellent precision.

Of course, almost all methods<sup>51</sup> for obtaining solutions to non-linear problems, including the one outlined in this work, rely on iterating from an initial set of estimates. The fact that the calculations eventually converge to a final value does not necessarily prove that another solution, with even smaller residual sums of squares, might not exist and be approachable from another set of initial estimates. However, for the problem described herein, the existence of more than one physically reasonable solution is remote since, at the initial values we tested, the nested and numerically-integrated GN computations converged to values similar to those used to create the data (*Figure 4*).

### Reaction progress curve modeling: observed data

A facile reaction progress curve-fitting routine, which estimates kinetic parameters for multiple substrates, could be useful for immobilized enzymes. Pseudo-zero order kinetic techniques require numerous independent observations of  $\rho$  as a function of the primary substrate concentration (with at least two secondary and tertiary substrate concentrations) and are not readily applicable<sup>47</sup> for enzymes immobilized on films,<sup>46</sup> sol-gel glasses,<sup>13,48</sup> non-woven fabrics<sup>7</sup> or microcapsular arrays.<sup>50</sup> In fact, we have found that, because of sampling error associated with a hydrated solid, the utilization of substrate saturation kinetics with Fractogel·GO results in somewhat unsatisfactory scatter (data not shown;  $K_G = 51$  mM,  $K_{O_2} = 694$   $\mu$ M). Using the nested and numerically-integrated GN procedure we obtained similar parametric estimates (*Figure 5A*:  $K_G = 67 \pm 15$  mM,  $K_{O_2} = 628 \pm 50$   $\mu$ M;  $\pm \varepsilon$ , the asymptotic standard

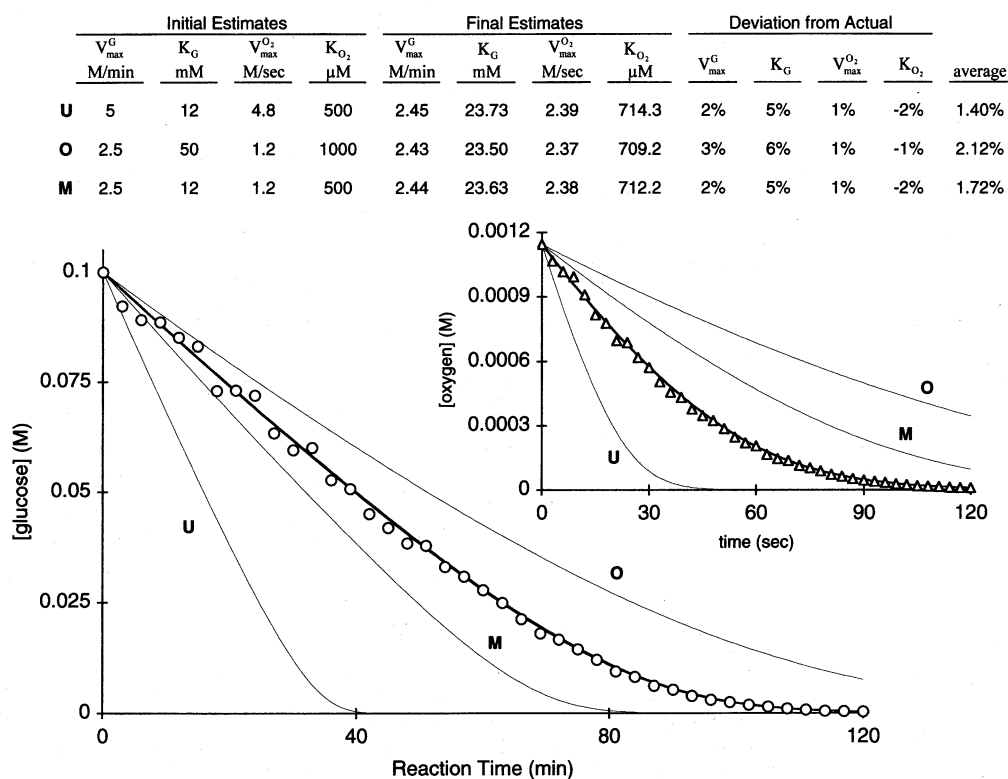


**Figure 4** Demonstration that, at various starting parametric estimates, the *nested* and numerically-integrated bimolecular ordered-sequential (bi-bi ping-pong) rate expression GN method converges to values similar to those (approx.  $\pm 6\%$ ) used to calculate the data ( $\pm 5\%$  random error). The final fits displayed in this figure resulted from the three calculated lines at the various starting conditions and demonstrate the high degree of precision obtained in these curve fits. In the inset table of initial/final estimates the first row of numbers represent initial values which cause the reaction progress curve fits to undershoot the observed (*U*), the second line of initial estimates cause the curves to overshoot (*O*) the observed while the third has mixed (*M*) values. Open circles represent [G] data; open triangles represent [O<sub>2</sub>] data. The light lines represent the curves for initial estimates of the parameters; the dark lines represent the final estimates

error<sup>51</sup>) and, simultaneously, predicted Fractogel·GO's reaction progress directly. *Figure 5B* shows traditional initial velocity kinetic data ( $\rho$  vs.  $[G]_0$  for air- and O<sub>2</sub>-saturated solutions) for GO type X-S in solution ( $K_G = 52 \pm 4$  mM,  $K_{O_2} = 721 \pm 61$   $\mu$ M) using non-linear regression analysis of Eq. (1a). Because our technique requires both primary and secondary substrate reaction progress data as a function of reaction time, so as to solve for  $K_G$  and  $K_{O_2}$  simultaneously, two  $V_{max}$  terms are obligatory ( $V_{max}^G$  and  $V_{max}^{O_2}$ ). Thus, two independent activity associated parameters were determined. From the glucose-O<sub>2</sub> reaction product data we found  $V_{max}^G$  and  $V_{max}^{O_2}$  were in good agreement [ $V_{max}^G = 36 \pm 4$  and  $V_{max}^{O_2} = 31 \pm 2$  units g<sup>-1</sup>; converted by a method similar to Eq. (4)] considering the disparity in amount of immobilized enzyme used (1.59 g vs. 33 mg [hydrated]), time scale (180 vs. 10 min) and total reaction volume (25 vs. 1.42 ml). All methods of analysis for soluble or immobilized GO type X-S were similar and indicate that our nested and numerically-integrated GN linearization procedure is reasonable for experimental purposes. These data also argue that the Fractogel immobilization matrix does not substantially change the various kinetic parameters. This latter find-

ing is not surprising since Fractogel's particle size is small and this material has been specifically designed for affinity chromatographic purposes where matrix interactions with small ligands are best minimized.

We have replicated the aforementioned reaction progress experiments twice using another form of GO (type II) which has slightly different solution kinetic characteristics. In these experiments the initial glucose concentrations were 0.1 and 0.2 M (*Figures 6 and 7*, respectively). Using the nested and numerically-integrated GN procedure (*Figure 6A*) we estimated that  $K_G = 32 \pm 19$  mM,  $K_{O_2} = 688 \pm 78$   $\mu$ M,  $V_{max}^G = 44 \pm 8$  (1.76 g total) and  $V_{max}^{O_2} = 48 \pm 3$  units g<sup>-1</sup> (61 mg total). Doubling the initial glucose concentration provided similar results (*Figure 7*:  $K_G = 31 \pm 26$  mM,  $K_{O_2} = 833 \pm 84$   $\mu$ M,  $V_{max}^G = 92 \pm 17$  [0.75 g total] and  $V_{max}^{O_2} = 94 \pm 5$  units g<sup>-1</sup> [11 mg total]). *Figure 6B* shows traditional initial velocity kinetic data ( $\rho$  vs.  $[G]_0$ ) for this form of GO in solution ( $K_G = 23 \pm 2$  mM,  $K_{O_2} = 423 \pm 41$   $\mu$ M) using direct non-linear regression analysis of Eq. (1a).

Direct comparison of our results (*Figures 5-7*) to literature values for solution or immobilized GO is problematic due to variability.<sup>7,8,10,11,15-17,46</sup> For instance, the apparent  $K_G$  for glucose (using MM kinet-

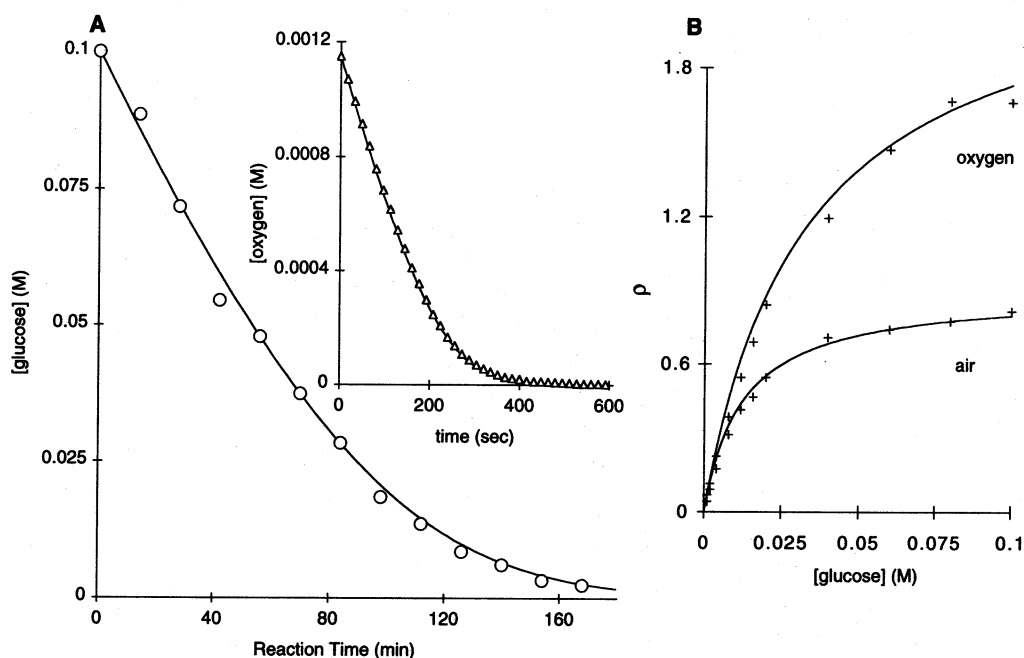


**Figure 5** (A) Primary substrate concentrations,  $[G]$  (open circles), plotted as a function of reaction time in the presence of Fractogel·GO (1.59 g Fractogel·GO [type X-S] hydrated matrix; 38 units  $g^{-1}$ ;  $\Delta t=14$  min). *Inset*: plot of the secondary substrate concentration ( $O_2$  saturated; open triangles) as a function of reaction time (33 mg Fractogel·GO [type X-S] hydrated matrix;  $\Delta t=16$  s). (B)  $\rho$  Dependence on  $[G]_0$  (air or  $O_2$ -saturated) for soluble GO (type X-S). All solid lines represent the final fit with a minimized sums of squares

ics: *Aspergillus niger* GO) has been found (temp.  $\sim 20$ – $25^\circ C$ ) to vary 2–33 mM for a sampling of various forms of immobilized GO ( $\bar{K}_G = 16 \pm 12$  mM). An even wider range in apparent  $K_G$  is observed for GO used

in solution studies ( $K_G = 6$ – $110$  mM;  $\bar{K}_G = 60 \pm 43$  mM). GO's MM kinetic parameters depend upon variables such as pH and  $[O_2]_0$  as well as the methods utilized (stopped-flow, spectroscopic turnover, etc.) to

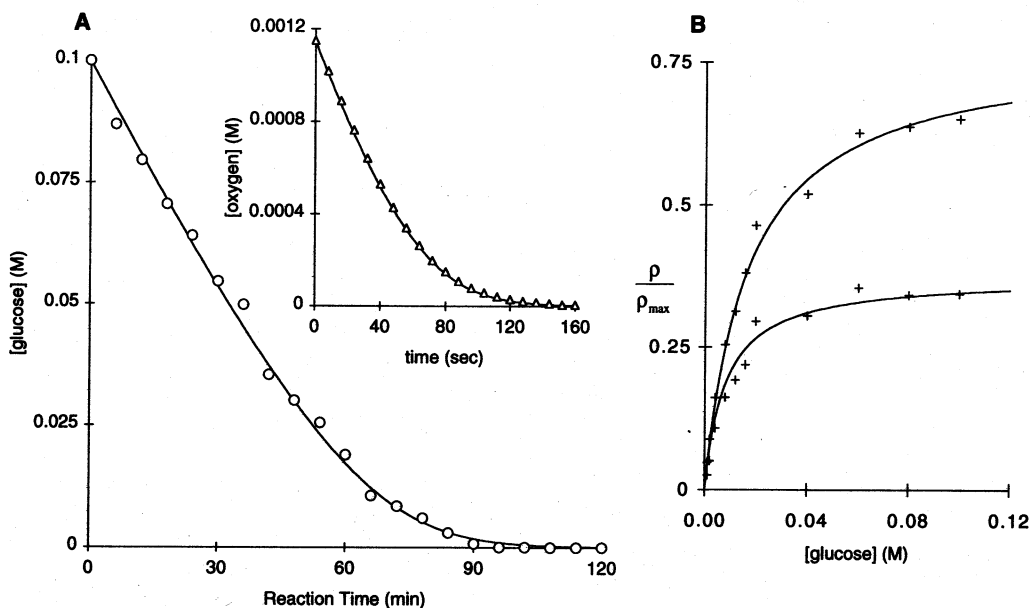


**Figure 6** (A) The dependence of  $[G]$  (open circles) on reaction time in the presence of Fractogel·GO (1.76 g Fractogel·GO hydrated [type II] matrix; 43 units  $g^{-1}$ ;  $\Delta t=6$  min). *Inset*: plot of the secondary substrate concentration ( $O_2$  saturated; open triangles) as a function of reaction time (61 mg Fractogel·GO hydrated [type II] matrix;  $\Delta t=8$  s). (B) Normalized  $\rho$  dependence on  $[G]_0$  (air or  $O_2$ -saturated) for soluble GO (type II); these data represent the mean of three observations. All solid lines represent the final fit with a minimized sums of squares

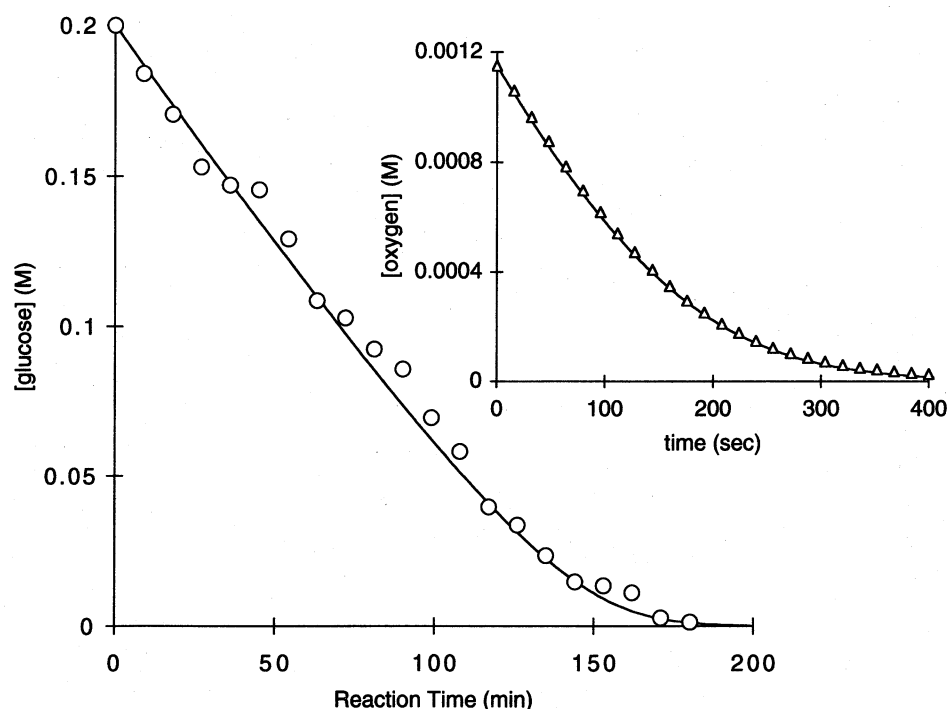


**Figure 7** Primary substrate concentrations (open circles),  $[G]_0 \sim 0.2$  M, plotted as a function of reaction time in the presence of Fractogel·GO (0.75 g Fractogel·GO [type III] hydrated matrix; 88 units  $g^{-1}$ ;  $\Delta t=9$  min). *Inset:* plot of the secondary substrate concentration ( $O_2$  saturated; open triangles) as a function of reaction time (11 mg Fractogel·GO [type III] hydrated matrix;  $\Delta t=16$  s). Solid lines represent the final fit with a minimized sums of squares

perform the kinetic analyses. Since the apparent  $K_G$  is modulated by the mechanism of substrate “delivery”<sup>23</sup> to the enzyme’s active site, small differences in ionic strength, viscosity of the medium, etc., could play a significant role in this observed kinetic inconstancy. Different forms of GO are also known to exist due, in part, to variance in carbohydrate content (six different forms) of the enzyme<sup>3,54</sup> and may explain the wide range in observed isoelectric points<sup>54</sup> ( $pI \sim 3.9-4.3$ ). In the studies reported herein, the apparent  $K_G$ s varied around 30 (type II) and 60 mM (type X-S) while  $K_{O_2}$ s were approximately 600–800  $\mu M$ .

## Conclusions

In this manuscript we have presented a method for estimating  $V_{max}^G$ ,  $V_{max}^{O_2}$ ,  $K_G$  and  $K_{O_2}$  (bi–bi ping-pong) from non-linear regression analysis of  $[G]$  and  $[O_2]$  as a function of reaction time in the presence of immobilized GO. We have made these analyses using nested GN linearization algorithms for the numerically-integrated PP rate expression on Microsoft EXCEL software. We applied this technique to realistic (e.g., with scatter) computer-generated reaction progress data and found that, with various starting conditions (initial parametric estimates), the calculations converged near to the parametric values used to create the data. Applying this technique with immobilized GO-catalyzed reac-

tions, we found that the enzyme’s kinetic parameters from curve fitting  $\rho$  as a function of variable  $[G]$  (two levels of  $[O_2]$ ) were similar to those determined employing the numerically-integrated PP rate expression. Lastly, our method was further tested by performing the analysis of reaction progress data at two different initial glucose concentrations which produced similar results to each other and indicated that  $K_G$ , from the nested and numerically-integrated ordered-sequential rate expression, is not dependent upon the starting conditions.

## References

1. Witteveen, C. F. B., Veenhuis, M., and Visser, J. Localization of glucose oxidase and catalase activities in *Aspergillus niger*. *Appl. Environ. Microbiol.* 1992, **58**, 1190–1194
2. Pazar, J. H., Kleepe, K., and Ball, E. M. The glycoprotein nature of some fungal carbohydrates. *Arch. Biochem. Biophys.* 1963, **103**, 515–518
3. Wilson, R., and Turner, A. P. F. Glucose oxidase: an ideal enzyme. *Biosensors Bioelectron.* 1992, **7**, 165–185
4. Hecht, H. J., Kalisz, H. M., Hendle, J., Schmid, R. D., and Schomburg, D. Crystal structure of glucose oxidase from *Aspergillus niger* refined at 2.3 Å resolution. *J. Mol. Biol.* 1993, **229**, 153–172
5. Keilin, D., and Hartree, E. F. The use of glucose oxidase (notatin) for the determination of glucose in biological material and for the study of glucose-producing systems by manometric methods. *Biochem. J.* 1948, **42**, 230–238
6. Turková, J., Vohník, S., Helusová, S., Benes, M. J., and Tichá, M. Galactosylation as a tool for the stabilization and immobilization of proteins. *J. Chromatog.* 1992, **597**, 19–27

## Papers

7. Asakura, T., Kitaguchi, M., Demura, M., Sakai, H., and Komatsu, K. Immobilization of glucose oxidase on nonwoven fabrics with *Bombyx mori* silk fibroin gel. *J. Appl. Polym. Sci.* 1992, **46**, 49–53
8. Arica, M. Y., and Hasirci, V. Immobilization of glucose oxidase: a comparison of entrapment and covalent bonding. *J. Chem. Technol. Biotechnol.* 1993, **58**, 287–292
9. Vassilev, N. B., Vassileva, M. Ch., and Spassova, D. I. Production of gluconic acid by *Aspergillus niger* immobilized on polyurethane foam. *Appl. Microbiol. Biotechnol.* 1993, **39**, 285–288
10. Elmgren, M., Lindquist, S.-E., and Sharp, M. Charge propagation through a redox polymer film containing enzymes—effects of enzyme loading, pH and supporting electrolyte. *J. Electroanal. Chem.* 1993, **362**, 227–235
11. Rishpon, J., Gottesfeld, S., Campbell, C., Davey, J., and Zamodzinski, T. A., Jr. Amperometric glucose sensors based on glucose oxidase immobilized in Nafion. *Electroanalysis* 1994, **6**, 17–21
12. Housaindokht, M. R., and Moosavi-Movahedi, A. A. Thermodynamic denaturation of glucose oxidase in aqueous dodecyl trimethyl ammonium bromide solution between 25 and 65°C. *Thermochim. Acta* 1994, **235**, 189–196
13. Heichal-Segal, O., Rappoport, T. S., and Braun, S. Immobilization in alginate-silicate sol-gel matrix protects  $\beta$ -glucosidase against thermal and chemical denaturation. *Biotechnology* 1995, **13**, 798–800
14. Keilin, D., and Hartree, E. F. Properties of glucose oxidase (notatin). *Biochem. J.* 1948, **42**, 221–229
15. Gibson, Q. H., Swoboda, B. E. P., and Massey, V. Kinetics and mechanism of action of glucose oxidase. *J. Biol. Chem.* 1964, **239**, 3927–3934
16. Swoboda, B. E. P., and Massey, V. Purification and properties of the glucose oxidase from *Aspergillus niger*. *J. Biol. Chem.* 1965, **240**, 2209–2215
17. Bright, H., and Gibson, Q. H. The oxidation of 1-deuterated glucose by glucose oxidase. *J. Biol. Chem.* 1967, **242**, 994–1003
18. Milsom, P., and Meers, J. *Comprehensive Biotechnology* (Moo-Young, M., Ed.). Pergamon Press, Oxford, UK, 1985, 681–700
19. Pierce, D. T., Unwin, P. R., and Bard, A. J. Scanning electrochemical microscopy. 17. Studies of enzyme-mediator kinetics for membrane- and surface-immobilized glucose oxidase. *Anal. Chem.* 1992, **64**, 1795–1804
20. Bright, H. J., and Porter, D. J. T. *The Enzymes* Vol. XII, Part B (Boyer, P. D., Ed.). Academic Press, New York, 1975, 421–466
21. Metzler, D. E. *Biochemistry: The Chemical Reactions of Living Cells*, Academic Press, New York, 1977, 301–352
22. Walsh, C. *Enzymatic Reaction Mechanisms*. W. H. Freeman & Co., San Francisco, 1979, 222–224
23. Gentry, R., Ye, L., and Nemerson, Y. A microscopic model of enzyme kinetics. *Biophys. J.* 1995, **69**, 356–361
24. Chaplin, M. G., and Bueke, C. *Enzyme Technology*, Cambridge University Press, Cambridge, UK, 1990, 80–13
25. Duggleby, R., and Morrison, J. Progress curve analysis in enzyme kinetics model discrimination and parameter estimation. *Biochim. Biophys. Acta* 1978, **526**, 398–409
26. Koerber, S., and Fink, A. The analysis of enzyme progress curves by numerical differentiation, including competitive product inhibition and enzyme reactivation. *Anal. Biochem.* 1987, **165**, 75–87
27. Schwert, G. W. The estimation of kinetic constants for the lactate dehydrogenase system by the use of integrated rate equations. *J. Biol. Chem.* 1969, **244**, 1285–1290
28. Yun, S.-L., and Suelter, C. H. A simple method for calculating  $K_m$  and  $V$  from a single enzyme reaction progress curve. *Biochim. Biophys. Acta* 1977, **480**, 1–13
29. Duggleby, R., and Morrison, J. The analysis of progress curves for enzyme-catalyzed reactions by non-linear regression. *Biochim. Biophys. Acta* 1977, **481**, 297–312
30. Duggleby, R. Estimation of the initial velocity of enzyme-catalyzed reactions by non-linear regression analysis of progress curves. *Biochem. J.* 1985, **228**, 55–60
31. Spector, T. Progress curve analysis of adenosine deaminase-catalyzed reactions. *Anal. Biochem.* 1984, **138**, 242–245
32. Duggleby, R. Progress-curve analysis in enzyme kinetics. *Biochem. J.* 1996, **235**, 613–615
33. Vandenberg, J., Kuchel, P., and King, G. Application of progress curve analysis to in situ enzyme kinetics using  $^1\text{H}$  NMR spectroscopy. *Anal. Biochem.* 1986, **155**, 38–44
34. Duggleby, R., and Clarke, R. Experimental designs for estimating the parameters of the Michaelis-Menton equation for progress curves of enzyme-catalyzed reactions. *Biochim. Biophys. Acta* 1991, **1080**, 231–236
35. Blée, E., and Schuber, F. Regio- and enantioselectivity of soybean fatty acid epoxide hydrolase. *J. Biol. Chem.* 1992, **267**, 11881–11887
36. Harjunpaa, V., Teleman, A., Koivula, A., Ruohonen, L., and Teeri, T. Cello-oligosaccharide hydrolysis by cellobiohydrolase II from *Trichoderma reesei*. *Eur. J. Biochem.* 1996, **240**, 584–591
37. Wimalasena, K., and Haines, D. A general progress curve method for the kinetic analysis of suicide enzyme inhibitors. *Anal. Biochem.* 1996, **234**, 175–182.
38. Cornish-Bowden, A. Analysis of progress curves in enzyme kinetics. *Biochem. J.* 1972, **130**, 637–639
39. Duggleby, R., and Morrison, J. Progress curve analysis of adenosine deaminase-catalyzed reactions. *Biochim. Biophys. Acta* 1979, **568**, 357–362
40. Dags, R., Pauliukonis, A., Kazlauskas, D., and Mankevicius, M. Determination of initial velocities of enzymatic reactions from progress curves. *Biochem. J.* 1986, **237**, 821–825
41. Visser, S., and Rollema, H. Quantification of chymosin action on nonlabeled  $\kappa$ -casein-related peptide substrates by ultraviolet spectrophotometry: description of kinetics by the analysis of progress curves. *Anal. Biochem.* 1986, **153**, 235–241
42. Bedino, S., Testore, G., and Obert, F. A simple steady state kinetic model for alcohol dehydrogenase: use of reaction progress curves for parameters estimation at pH 7.4. *Ital. J. Biochem.* 1987, **36**, 243–255
43. Jennings, R. R., and Niemann, C. The evaluation of the kinetic constants of enzyme-catalyzed reactions by procedures based upon integrated rate equations. *J. Am. Chem. Soc.* 1955, **77**, 5432–5433
44. Alberty, R. A., and Koerber, B. B. Studies of the enzyme fumarase. VII. Series solutions of integrated rate equations for irreversible and reversible Michaelis-Menten mechanisms. *J. Am. Chem. Soc.* 1957, **79**, 6379–6382
45. Irwin, P., Damert, W., and Doner, L. Curve fitting in nuclear magnetic resonance spectroscopy: illustrative examples using a spreadsheet and microcomputer. *Concepts Magn. Res.* 1994, **6**, 57–67
46. Fortier, G., and Bélanger, D. Characterization of the biochemical behavior of glucose oxidase entrapped in a polypyrrole film. *Biotechnol. Bioeng.* 1991, **37**, 854–858
47. Kierstan, M. P. J., and Coughlan, M. P. Immobilization of proteins by noncovalent procedures: principles and applications. *Bioprocess Technol.* 1991, **14**, 13–71
48. Shtelzen, S., Rappoport, S., Avnir, D., Ottolenghi, M., and Braun, S. Properties of trypsin and of acid phosphatase immobilized in sol-gel glass matrices. *Biotechnol. Appl. Biochem.* 1992, **15**, 227–235
49. Edmiston, P. L., Wambolt, C. L., Smith, M. K., and Saavedra, S. S. Spectroscopic characterization of albumin and myoglobin entrapped in bulk sol-gel. *J. Colloid Interface Sci.* 1994, **163**, 395–406
50. Parthasarathy, R. V., and Martin, C. R. Synthesis of polymeric microcapsule arrays and their use for enzyme immobilization. *Nature* 1994, **369**, 298–301
51. Draper, N., and Smith, H. *Applied Regression Analysis*, 2nd Ed., John Wiley and Sons, New York, 1981, 462–465
52. Wider, G., and Wüthrich, K. *J. Magn. Res.* 1993, **103**, 239–241
53. Pfeffer, P. E., Valentine, K. M., and Parrish, F. W. Deuterium-induced differential isotope shift  $^{13}\text{C}$  NMR. 1. Resonance reassignments of mono- and disaccharides. *J. Am. Chem. Soc.* 1979, **101**, 1265–1274
54. Hayashi, S., and Nakamura, S. Multiple forms of glucose oxidase with different carbohydrate compositions. *Biochim. Biophys. Acta* 1981, **657**, 40–51